

# Online Research @ Cardiff

This is an Open Access document downloaded from ORCA, Cardiff University's institutional repository: <https://orca.cardiff.ac.uk/id/eprint/123425/>

This is the author's version of a work that was submitted to / accepted for publication.

Citation for final published version:

Permyakov, Eugene A., Turner, Matthew, Mutter, Shaun T., Kennedy-Britten, Oliver D. and Platts, James A. ORCID: <https://orcid.org/0000-0002-1008-6595>  
2019. Molecular dynamics simulation of aluminum binding to amyloid- $\beta$  and its effect on peptide structure. PLoS ONE 14 (6) , e0217992.  
10.1371/journal.pone.0217992 file

Publishers page: <http://dx.doi.org/10.1371/journal.pone.0217992>  
<<http://dx.doi.org/10.1371/journal.pone.0217992>>

Please note:

Changes made as a result of publishing processes such as copy-editing, formatting and page numbers may not be reflected in this version. For the definitive version of this publication, please refer to the published source. You are advised to consult the publisher's version if you wish to cite this paper.

This version is being made available in accordance with publisher policies.

See

<http://orca.cf.ac.uk/policies.html> for usage policies. Copyright and moral rights for publications made available in ORCA are retained by the copyright holders.

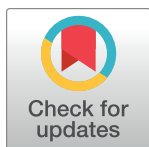


## RESEARCH ARTICLE

# Molecular dynamics simulation of aluminium binding to amyloid- $\beta$ and its effect on peptide structure

Matthew Turner, Shaun T. Mutter, Oliver D. Kennedy-Britten, James A. Platts<sup>\*</sup>

School of Chemistry, Cardiff University, Park Place, Cardiff, United Kingdom

<sup>\*</sup> [platts@cardiff.ac.uk](mailto:platts@cardiff.ac.uk)


## Abstract

Multiple microsecond-length molecular dynamics simulations of complexes of Al(III) with amyloid- $\beta$  (A $\beta$ ) peptides of varying length are reported, employing a non-bonded model of Al-coordination to the peptide, which is modelled using the AMBER ff14SB forcefield. Individual simulations reach equilibrium within 100 to 400 ns, as determined by root mean square deviations, leading to between 2.1 and 2.7  $\mu$ s of equilibrated data. These reveal a compact set of configurations, with radius of gyration similar to that of the metal free peptide but larger than complexes with Cu, Fe and Zn. Strong coordination through acidic residues Glu3, Asp7 and Glu11 is maintained throughout all trajectories, leading to average coordination numbers of approximately 4 to 5. Helical conformations predominate, particularly in the longer Al-A $\beta$ 40 and Al-A $\beta$ 42 peptides, while  $\beta$ -strand forms are rare. Binding of the small, highly charged Al(III) ion to acidic residues in the N-terminus strongly disrupts their ability to engage in salt bridges, whereas residues outside the metal binding region engage in salt bridges to similar extent to the metal-free peptide, including the Asp23-Lys28 bridge known to be important for formation of fibrils. High helical content and disruption of salt bridges leads to characteristic tertiary structure, as shown by heat maps of contact between residues as well as representative clusters of trajectories.

## OPEN ACCESS

**Citation:** Turner M, Mutter ST, Kennedy-Britten OD, Platts JA (2019) Molecular dynamics simulation of aluminium binding to amyloid- $\beta$  and its effect on peptide structure. PLoS ONE 14(6): e0217992. <https://doi.org/10.1371/journal.pone.0217992>

**Editor:** Eugene A. Permyakov, Russian Academy of Medical Sciences, RUSSIAN FEDERATION

**Received:** March 28, 2019

**Accepted:** May 23, 2019

**Published:** June 11, 2019

**Copyright:** © 2019 Turner et al. This is an open access article distributed under the terms of the [Creative Commons Attribution License](https://creativecommons.org/licenses/by/4.0/), which permits unrestricted use, distribution, and reproduction in any medium, provided the original author and source are credited.

**Data Availability Statement:** Data generated in this study, in the form of MD trajectories and coordinates for clusters, in PDB format, are available from Zenodo DOI: [10.5281/zenodo.2605360](https://doi.org/10.5281/zenodo.2605360).

**Funding:** This work was funded by the UK Engineering and Physical Sciences Research Council under grant ref EP/N016858/1, awarded to JAP. The funder had no role in study design, data collection and analysis, decision to publish, or preparation of the manuscript.

## Introduction

Alzheimer's disease (AD) is a devastating neurodegenerative condition that poses major healthcare challenges. Significant hallmarks of AD include the death of neurons and their connections in addition to the presence of insoluble plaques and neurofibrillary tangles. The amyloid hypothesis suggests that aggregation of the amyloid- $\beta$  (A $\beta$ ) peptide into soluble oligomers and senile plaques is the main driver of AD.[1,2] In contrast, the metal ion hypothesis suggests that disruption of metal ion homeostasis promotes A $\beta$  aggregation and onset of AD.[3–5] The primary focus of the metal ion hypothesis has been on naturally occurring metals, particularly Cu(II),[6–11] Zn(II),[12–15] and Fe(II),[16–20] though studies over several decades have also linked aluminium(III) with the development of AD.[21–25] Aluminium does not naturally occur in human biology, but Al(III) is a known neurotoxin that interacts with a range of

**Competing interests:** The authors have declared that no competing interests exist.

metal-binding proteins, influencing the homeostasis of other ions. Specifically, Exley et al showed that aluminium induces conformational changes in A $\beta$ , [26] that have been linked to inhibition of A $\beta$  degradation as well as promotion of aggregation, [27] and formation of reactive oxygen species. [28]

To date, several simulation studies on the interaction of aluminium with A $\beta$  have been reported, focussing on the binding modes of Al(III) with A $\beta$  and the resulting morphology of Al-A $\beta$  aggregates. [29,30] Recently, Mujika et al used a computational approach to generate 3D models of Al(III) bound to the N-terminal A $\beta$ 16 fragment of A $\beta$  in a 1:1 stoichiometry. [31] Here, Al shows a clear preference for coordination by carboxylate groups (Glu3, Asp7 and Glu11) with the remaining coordination sites occupied by backbone carbonyl moieties or water molecules. In addition, the authors performed molecular dynamics (MD) simulations of the resulting complexes. These validated their identified coordination modes, but were too short to properly sample the ensemble of structures available to such complexes due to the inherently flexible and disordered nature of A $\beta$ . In this context, we note that a recent study has compared the effect of Li, Na and K ions on A $\beta$  structure and stability. [32]

In order to examine Al-A $\beta$  interactions in more detail, as well as their effect on peptide structure, we report MD simulations of Al(III) interacting with the N-terminal A $\beta$ 16 fragment as well as the full A $\beta$ 40 and A $\beta$ 42 peptides, using molecular mechanics incorporating a non-bonded model of Al(III) coordination. In this way, we aim to sample a wide range of conformations of the intrinsically disordered A $\beta$  peptide as well as allowing Al(III) to sample a range of coordination sites in the peptide.

## Computational methods

A $\beta$  peptides were constructed in extended conformations in MOE [33] with appropriate residue protonation states for physiological pH. Al(III) was coordinated via Glu3, Asp7 and Glu11, as identified by Mujika et al. [31] Structures were subjected to short LowMode [34] conformational searches to obtain reasonable starting structures. MD simulations were performed using the AMBER16 package. [35] The AMBER ff14SB forcefield parameter set [36] was used to model all standard amino acid residues; the non-bonded MCPB.py [37] approach was used for Al(III), enabling the metal ion to sample different coordination sites during simulation. RESP charges for the metal-coordinating regions were obtained from B3LYP/6-31G(d) calculations using Gaussian09. [38] This combination of functional and basis set matches that used by Li and Merz in developing and testing MCPB.py, and is recommended for compatibility with AMBER-style forcefields. The Al(III) ion was fixed as a 3+ charge, with radius of 1.37 Å.

The Generalised Born solvation model was used to solvate all Al(III)-A $\beta$  systems, [39] as this has been shown to enhance sampling of flexible systems. [40] MD simulations were carried out in the NVT ensemble, using the Langevin thermostat to control temperature. The SHAKE algorithm was used to constrain bonds to hydrogen, and simulations performed using a 2 fs integration timestep. Analysis of the trajectories was performed using CPPTRAJ v16.16 [41] and VMD 1.9.3. [42] Secondary structure assignment was made using the DSSP algorithm [43] in CPPTRAJ. Salt bridges were defined as any contact distance of less than 3.2 Å between oxygen and nitrogen atoms in charged residues. Clustering used the DBSCAN algorithm of Ester et al. [44] Ramachandran maps and hydrogen bonding plots were made using MDplot. [45]

## Results

Three separate 1  $\mu$ s simulations of Al-A $\beta$ 16 (denoted A, B and C) were performed, starting from the same minimised conformation, but with different random velocities sampled from the Maxwell-Boltzmann distribution at 310 K. Similarly, five 1  $\mu$ s simulations (A-E) were

performed for both Al-A $\beta$ 40 and Al-A $\beta$ 42. Root mean square displacement (RMSD) relative to the starting structures was used as a measure of equilibration.[9,46] Fig 1 shows RMSD plots for all backbone atoms in Al-A $\beta$ 16, Al-A $\beta$ 40 and Al-A $\beta$ 42 systems, respectively, relative to their respective minimised structures. Equilibration points are shown in Table 1; Al-A $\beta$ 16 simulations reach stable values rapidly, while Al-A $\beta$ 40 and Al-A $\beta$ 42 simulations take longer to equilibrate. All analysis reported is taken from data extracted from frames after each equilibration point, averaged over the relevant simulations, such that trajectories of 2.7, 2.1 and 2.4  $\mu$ s are available for further analysis. Averages and standard deviations of RMSD are shown in Table 2, further illustrating the equilibration of the trajectories: standard deviations of around 1 Å are found across the multiple microsecond trajectories. As might be expected, the larger peptides reach larger average values of RMSD than the N-terminal fragment, with a notable increase for the 42-residue peptide over the 40-residue one.

In principle, the non-bonded model of Al(III) coordination used allows the ion to sample alternative donor atoms than the carboxylate sidechains at which simulations were started. All Al—O distances were monitored over all equilibrated frames for Al-A $\beta$ 42, from which it is clear that the anionic Glu3, Asp7 and Glu11 residues dominate binding. Distances of  $1.858 \pm 0.036$  Å for Glu3 sidechain O,  $1.813 \pm 0.030$  Å for Asp7 sidechain O, and  $2.615 \pm 0.865$  Å and  $2.917 \pm 0.887$  Å for each carboxylate O in Glu11 sidechain are recorded. This indicates that mono-dentate binding prevails for Glu3 and Asp7, whereas Glu11 binds more in bi-dentate fashion. Transient Al—O contacts are also observed for backbone O of Glu3 (minimum 1.769, mean 4.440 Å) and Phe4 (minimum 3.313, mean 7.457 Å) are also observed.

Summing across all oxygen atoms for all frames in the equilibrated Al-A $\beta$ 42 trajectory leads to the radial distribution function (RDF) for ion coordination, as shown in Fig 2A. RDFs for smaller peptides (reported in ESI) are similar. A single sharp peak centred on 1.9 Å corresponds to dominant sidechain coordination, while a lower and broader feature around 3.8 Å

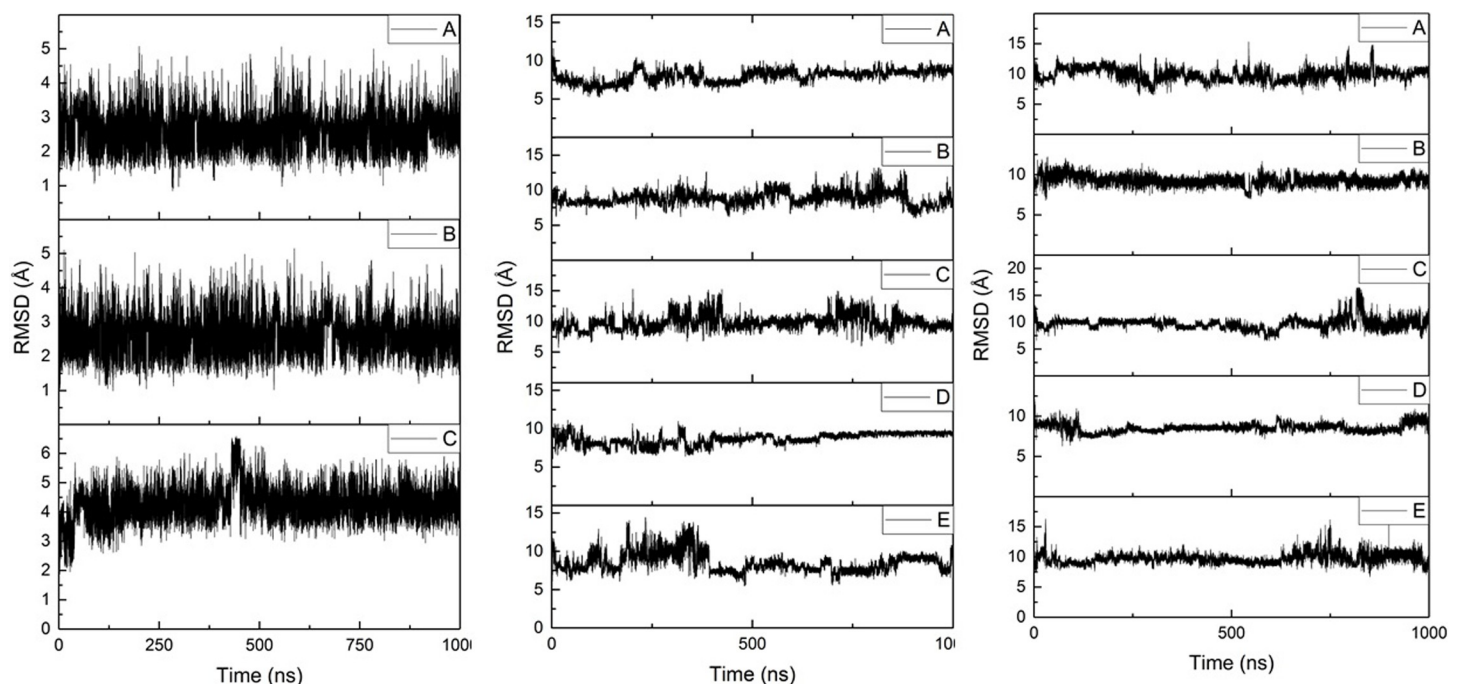


**Fig 1. Backbone RMSD for simulations of Al-A $\beta$ 16, Al-A $\beta$ 40 and Al-A $\beta$ 42.**

<https://doi.org/10.1371/journal.pone.0217992.g001>



**Table 1. Equilibration point for simulations (ns).**

	Al-A $\beta$ 16	Al-A $\beta$ 40	Al-A $\beta$ 42
A	100	480	320
B	100	50	200
C	125	400	100
D		100	240
E		400	200

<https://doi.org/10.1371/journal.pone.0217992.t001>

shows evidence for some outer-sphere interaction. Integrating the RDF (Fig 2B) leads to an average coordination number of 3.7 for Al.

Radius of gyration (Rg) values show similar trends to RMSD; plots of Rg as a function of simulation time are shown in Fig 3 and summary statistics in Table 3. Al-A $\beta$ 16 displays the smallest average Rg (*ca.* 8 Å) among the systems studied, while the much longer Al-A $\beta$ 40 and Al-A $\beta$ 42 peptides exhibit only slightly larger average Rg values (*ca.* 10.6 and 11.6 Å, respectively), suggesting that the larger peptides adopt collapsed rather than extended conformations in the presence of Al(III). For comparison, Rg values of 13.1 Å (using AMBER ff03) and 10.1 Å (using AMBER ff99SB) have been reported in literature for the metal-free A $\beta$ 42.[9,47] Rg values for Cu, Fe and Zn bound to A $\beta$ 16 and sampled in similar manner[48] were 7.6, 7.2 and 8.1 Å, respectively, indicating that Al(III) coordination leads to less compact structures than do those metals.

Root-mean-square fluctuation (RMSF) values for individual residues are shown in Fig 4, with associated data in Supporting Information. For Al-A $\beta$ 16, both termini (Asp1 and His13-Lys16) are flexible with RMSF values > 4.0 Å, whereas Ala2, Ser8, Glu11 and Val12 are the least flexible residues (RMSF < 2.5 Å). Interestingly, the metal binding residues Glu3 and Asp7 exhibit greater fluctuation than their neighbours, in contrast to previous work using an explicit metal-ligand bonding terms within the molecular mechanics energy expression.[48] In the larger peptide systems, different patterns of residue flexibility are observed: in both cases, Glu11 stands out as particularly stable, while other coordinating residues are also relatively inflexible. The anchoring effect of coordination extends beyond individual residues to encompass the whole of the Asp7-Glu11 segment (RMSF < 3.6 Å), whereas Arg5 is highly mobile in both cases. In addition, residues corresponding to the central hydrophobic core (CHC, *i.e.* Leu17 to Ala21) and the C-terminus are found to undergo large fluctuations, reflecting the expected unstructured nature of the single peptide in aqueous conditions. In both cases, Gly33 has relatively low RMSF: as a small residue close to the C-terminus, this might be expected to be highly mobile. Further analysis (*vide infra*) indicates this residue is involved in hydrogen bonding. The final two residues of A $\beta$ 42 are particularly mobile, indicating a lack of structure of the C-terminus in the larger peptide and contributing to the larger overall RMSD noted above.

Secondary structure adopted by A $\beta$ , and the effect of Al-binding on this, is a key aspect of the metal hypothesis for AD. Fig 5 shows the Ramachandran maps that result from post-equilibration MD trajectories for all three peptides bound to Al(III), showing that the peptides

**Table 2. RMSD statistics for post-equilibration simulations (Å).**

	Ave	SD	Min	Max
A $\beta$ 16	3.19	0.93	0.85	6.59
A $\beta$ 40	8.78	1.15	1.91	15.26
A $\beta$ 42	9.43	0.91	6.52	16.46

<https://doi.org/10.1371/journal.pone.0217992.t002>

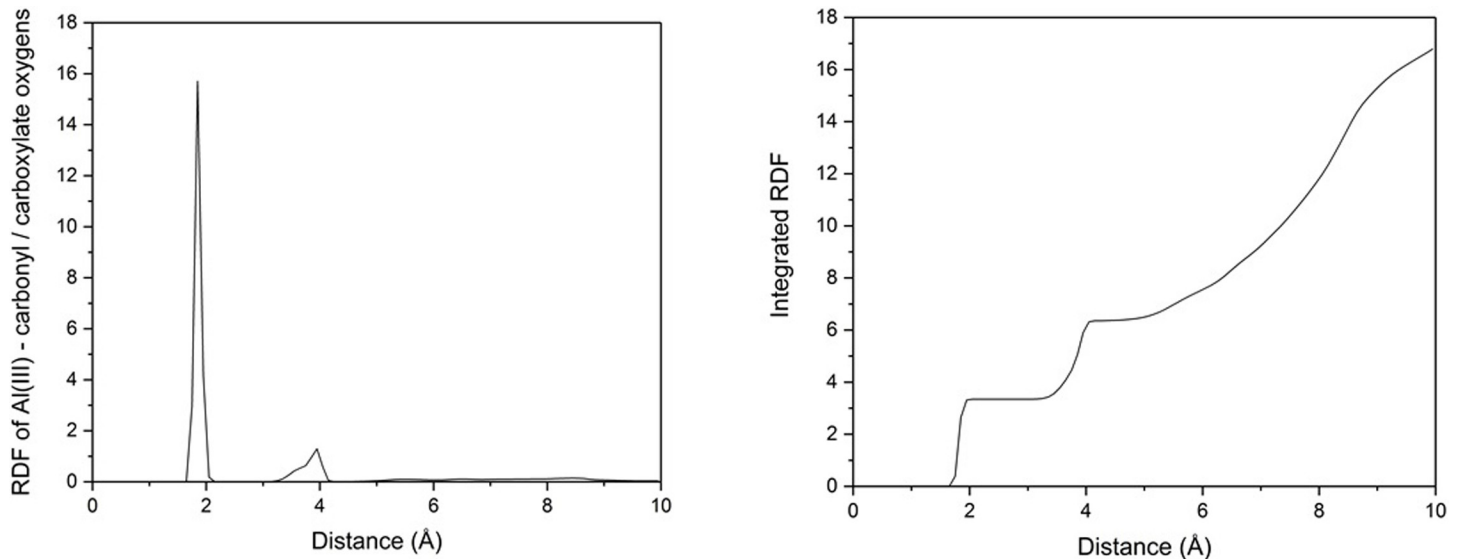


Fig 2. (a) RDF and (b) integrated RDF of Al-oxygen distances in Al-A $\beta$ 42.

<https://doi.org/10.1371/journal.pone.0217992.g002>

spend most time in the general region of  $\alpha$ -helices, with smaller but noticeable populations of  $\beta$ -strand, poly-proline II and left-handed helix regions and a rather broad distribution in  $\phi/\Psi$  space. The relative significance of the non- $\alpha$ -helix regions diminishes in the larger peptides compared to Al-A $\beta$ 16. These observations can be quantified by assignment of secondary structure using DSSP, as summarised in Fig 6. This shows that coil/turn/bend structures predominate in the N-terminal region, along with a smaller contribution from 3<sub>10</sub> and  $\alpha$ -helices. Key metal-binding residues 3, 7 and 11 do not have noticeably different secondary structure from the rest of the N-terminus, nor from previous reports for metal-free A $\beta$ 42. Helical content

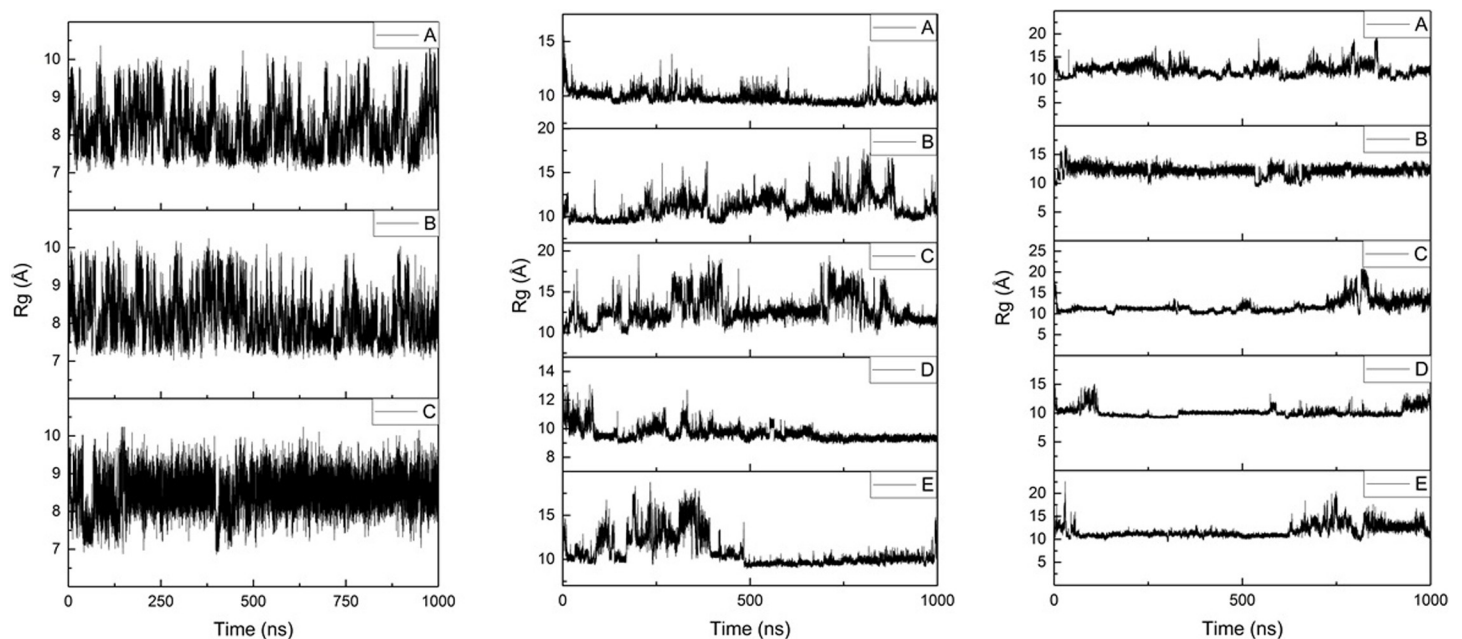


Fig 3. Rg plots for Al-A $\beta$ 16, Al-A $\beta$ 40 and Al-A $\beta$ 42 simulations.

<https://doi.org/10.1371/journal.pone.0217992.g003>

Table 3. Rg statistics for post-equilibration simulations (Å).

	Ave	SD	Min	Max
Aβ16	8.24	0.59	6.86	10.30
Aβ40	10.59	1.52	8.89	19.44
Aβ42	11.58	1.41	8.97	20.92

<https://doi.org/10.1371/journal.pone.0217992.t003>

increases beyond the immediate N-terminus, although significant amounts of 3<sub>10</sub> and  $\alpha$ -helix are apparent in Glu11-Lys16 in all systems. The CHC exhibits relatively few helical residues, and also a small amount of  $\beta$ -strand, which is mostly antiparallel in AI-Aβ40 but parallel in AI-Aβ42. Helical content then increases toward the C-terminus, reaching maximal values in the sequence Ala30 to Val36, while the final few residues of both peptides are rather unstructured. Values summed across the entire peptides are reported in Table 4, and show increasing amounts of helical content as the peptide elongates. Even for AI-Aβ16, 30% of residues are classified as helical, rising to almost 40% of AI-Aβ40 and nearly 50% of AI-Aβ42. Fig 6, along with visualisation of representative clusters of trajectories (*vide infra*), shows that this helical character does not take the form of a single helix, but rather of several short (4 to 8 residue) segments with helical form.

Table 5 shows statistics relating to the number of hydrogen bonds present over equilibrated simulations. Aβ16 has approximately four hydrogen bonds per simulation frame, although the standard deviation value suggests that these interactions are transitory; this system also contains frames with as many as 14, or as few as zero hydrogen bond interactions. Aβ40 contains, on average, just less than twelve hydrogen bonds per frame: again this covers great variability with as many as 26 simultaneous hydrogen bonds, as well as frames with none. Aβ42 contains almost 14 hydrogen bonds per simulation frame, on average, with as few as 2 or as many as 32 hydrogen bonds present in a given frame. The specific identities and prevalence of these interactions are shown in Fig 7. In AI-Aβ16, there are 471 different hydrogen bond interactions present for at least 1 frame; the most common (reported as donor-acceptor) are between Gly9 backbone-His6 backbone (20.7%), His14 sidechain-Glu11 backbone (14.0%) and Gln15 backbone-Val12 backbone (13.2%). There are twelve i+4  $\rightarrow$  i backbone-backbone hydrogen bonds, characteristic of  $\alpha$ -helices, though only three are present for more than 5% of simulation. Similarly, there are 13 i+3  $\rightarrow$  i hydrogen bonds (typical of 3<sub>10</sub>-helices) and 8 i+5  $\rightarrow$  i interactions ( $\pi$ -helices), though only 4 and 2, respectively, are present for 5% or more of simulation time.

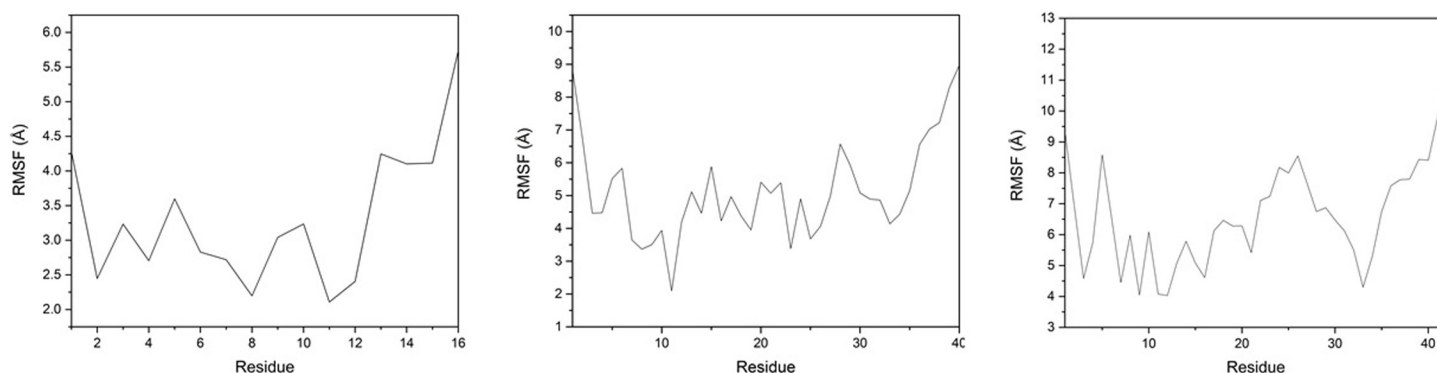
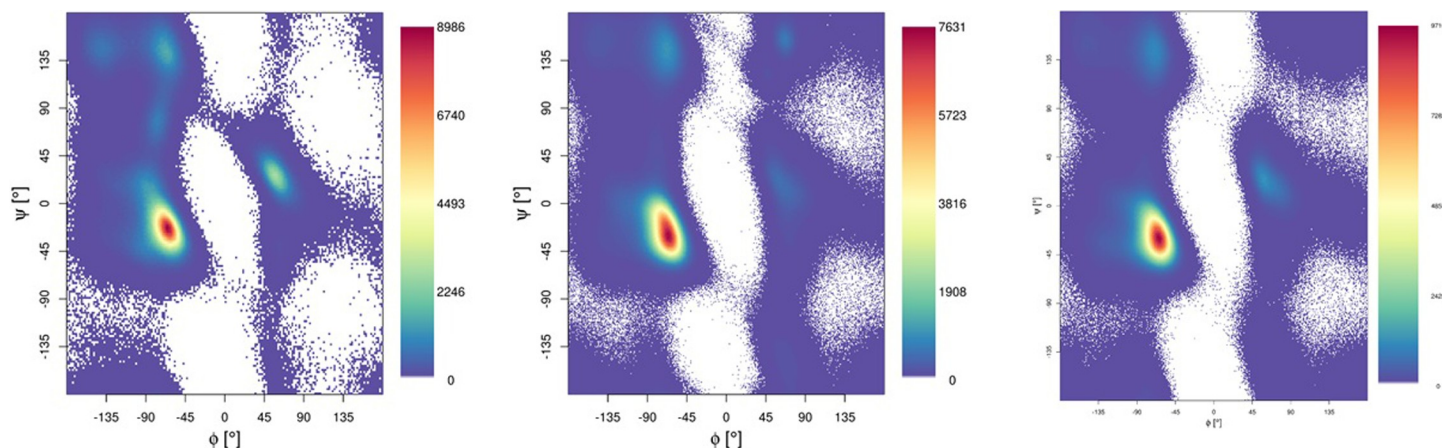


Fig 4. RMSF plots, by residue, for AI-Aβ16, AI-Aβ40 and AI-Aβ42.

<https://doi.org/10.1371/journal.pone.0217992.g004>



**Fig 5.** Ramachandran plots for simulations of Al-A $\beta$ 16, Al-A $\beta$ 40 and Al-A $\beta$ 42.

<https://doi.org/10.1371/journal.pone.0217992.g005>

In Al-A $\beta$ 40 there are 1807 different hydrogen bonds observed, the most prevalent being His14 sidechain-Tyr10 backbone (33.4%), Glu11 backbone-Glu11 sidechain (28.1%) and His13 sidechain-Gly9 backbone (20.9%). Of these, 32 are  $i+4 \rightarrow i$  backbone-backbone hydrogen bonds, of which 15 are present for more than 5% of simulation; notable contributions are made by Ile32-Val36 (18.9%) and Ile31-Met35 (15.2%). Furthermore, there are 14  $i+3 \rightarrow i$  and just 1  $i+5 \rightarrow i$  interactions present in excess of 5% of simulation, reflecting the greater contribution of  $\alpha$ -helices. The hydrogen bonding pattern is similar A $\beta$ 42, common contacts include Glu11 backbone-Glu11 sidechain (53.1%), His14 sidechain-Tyr10 backbone (27.4%) and Asp7 backbone-Glu3 backbone (22.4%). In total, 1688 hydrogen bonds are observed; 19  $i+4 \rightarrow i$  hydrogen bonds, 16  $i+3 \rightarrow i$  hydrogen bonds and 2  $i+5 \rightarrow i$  hydrogen bonds each over 5% occupancy.

Salt bridge interactions also play an important role in the stability of amyloid- $\beta$  structures. The incidence of these interactions is summarised in Fig 8. In A $\beta$ 16, there are eight possible salt bridges, five of which are occupied for at least 1% of total simulation time. Of these, the most common are Asp1-Arg5 (54%), followed by Glu11-Arg5 (20%). Interestingly, Asp1 and Glu11 form more salt bridges than Glu3 and Asp7. This may be because the more central Glu3 and Asp7 residues are commonly involved in coordination of Al, such that their charged sidechains are less available for salt bridge formation. In A $\beta$ 40 and A $\beta$ 42, there are eighteen possible salt bridges: A $\beta$ 40 has the greater range of salt bridge interactions, with eleven present for

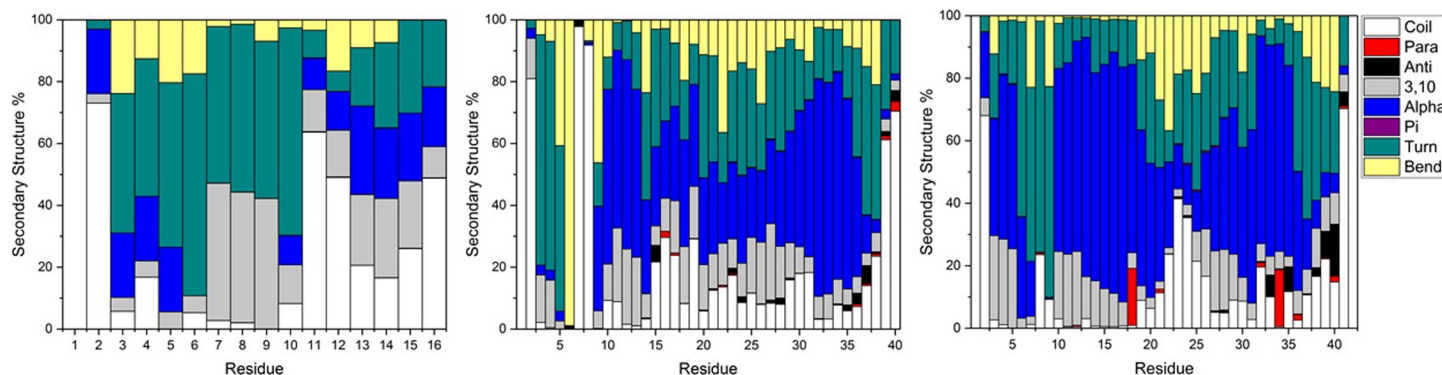


**Fig 6.** Peptide secondary structure percentage, by residue, for Al-A $\beta$ 16, Al-A $\beta$ 40 and Al-A $\beta$ 42.

<https://doi.org/10.1371/journal.pone.0217992.g006>



**Table 4. Total secondary structure character for Al-A $\beta$ 16, Al-A $\beta$ 40 and Al-A $\beta$ 42.**

	Helix	Sheet	Other
A $\beta$ 16	30.2	0.0	69.8
A $\beta$ 40	39.4	1.1	59.4
A $\beta$ 42	48.2	2.3	49.5

<https://doi.org/10.1371/journal.pone.0217992.t004>

at least 1% of simulation time. The most common is Asp23-Arg5 (51%), with Asp1-Arg5 interaction also frequently observed (32%). Asp7 also forms numerous salt bridges (with Lys16: 24%, Lys28: 12%). However, the A $\beta$ 42 salt bridge network is notably different from Al-A $\beta$ 40; just seven of the eighteen possible interactions are present. Asp1-Arg5 is the most frequent interaction (43%), while Asp23-Lys28 is also prevalent (37%), but here Asp7 is not involved in any bridges.

Tertiary structure of the Al-A $\beta$  complexes are summarised using the C $\alpha$ -C $\alpha$  contact maps, as shown in Fig 9. Al-A $\beta$ 16 exhibits short contacts between Glu3-Phe4 and Glu11-His13, apparently driven by the constraints of metal coordination as well as the Arg5-Glu11 salt bridge. The same pattern is also present in Al-A $\beta$ 40 and Al-A $\beta$ 42. Al-A $\beta$ 40 also exhibits close contacts between Phe4-Arg5 and Glu22-Gly25, due to the prevalence of salt bridges to Glu22 and Asp23 in this system. The reduced incidence of these salt bridges in the longer Al-A $\beta$ 42 means that short contacts of the N-terminus with the central are much less evident here. Both longer peptides also have notable short contacts of Gly33 with Lys16-Ala21, *i.e.* central hydrophobic cluster, giving rise to the low RMSF observed for this residue.

Clusters were extracted from equilibrated trajectories: for Al-A $\beta$ 16 the most populated cluster is present for 25.4% of frames. As shown in Fig 10, this cluster is made up of coil in the N-terminal region, a turn centred on Gly9, and a helical section at the C-terminus, with Al(III) bound through backbone and sidechain O of Glu3 and Glu11 as well as sidechain of Asp7. Small elements of helical content are apparent between Asp7 and Glu11, and also at the C-terminal Lys16. The same process leads to less populated clusters for the longer peptides, indicating their more unstructured nature: the most populated clusters for Al-A $\beta$ 40 and Al-A $\beta$ 42 occupy just 4.1% and 2.5% of simulation time, with no other cluster accounting for as much as 1%. In both cases, a relatively unstructured N-terminus binds Al(III) through acidic sidechains. The Al-A $\beta$ 40 cluster is quite unstructured over the whole sequence, with small elements of helical structure in both the CHC and C-terminus, but neither extending over more than a handful of residues. In contrast, Al-A $\beta$ 42 includes an  $\alpha$ -helix over Glu11-Phe20, followed by a turn centred on Ala21 and a relatively unstructured C-terminus.

## Discussion

Microsecond timescale simulations of Al(III) bound to A $\beta$ 16, A $\beta$ 40 and A $\beta$ 42 in implicit aqueous solvent reveal a picture of a flexible, unstructured set of systems in which no one structure dominates. Equilibration, as judged by time evolution of RMSD, is fast for the smallest peptide, but takes several hundred nanoseconds for the larger ones. The non-bonded model of ion

**Table 5. Hydrogen bond statistics for Al-A $\beta$ 16, Al-A $\beta$ 40 and Al-A $\beta$ 42 simulations.**

	Ave	SD	Min	Max
A $\beta$ 16	4.13	1.79	0	14
A $\beta$ 40	11.96	3.04	0	26
A $\beta$ 42	13.70	3.44	2	32

<https://doi.org/10.1371/journal.pone.0217992.t005>

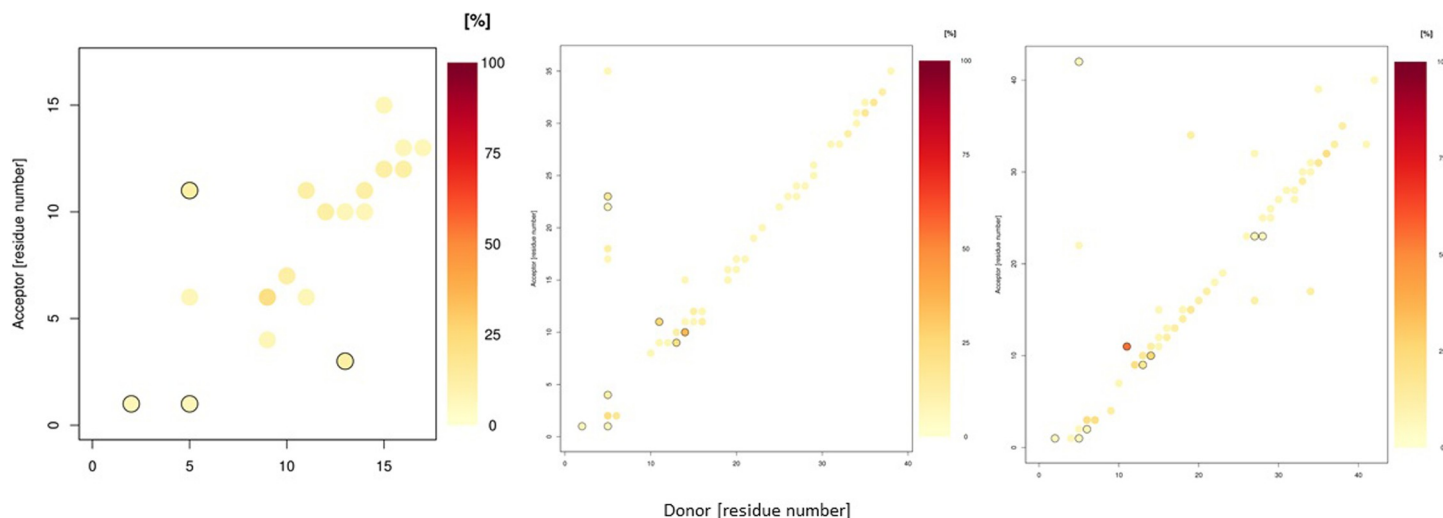


**Fig 7. Hydrogen bond incidence plots for Al-Aβ16, Al-Aβ40 and Al-Aβ42 simulations.** Black circles indicate more than one type of hydrogen bond between the relevant residues.

<https://doi.org/10.1371/journal.pone.0217992.g007>

coordination employed allows the ion to sample numerous ligating sites within the peptide, but in fact we find that coordination to the N-terminal acidic residues Glu3, Asp7 and Glu11 is highly stable across over 2  $\mu$ s of MD trajectories for each system. This leads to average coordination number in the inner coordination shell for Al of around 4, with a further 2 to 3 oxygens in the outer coordination shell.

Al-Aβ16 is a useful, computationally tractable model for metal coordination, but termination just beyond the metal binding N-terminus means that some properties are notably different between this and the full-length peptides. Nevertheless, some observations can be made for all three systems, in particular the relative lack of helical/sheet secondary structure in the N-terminus, low RMSF for metal-binding residues Glu3, Asp7 and Glu11, and the high

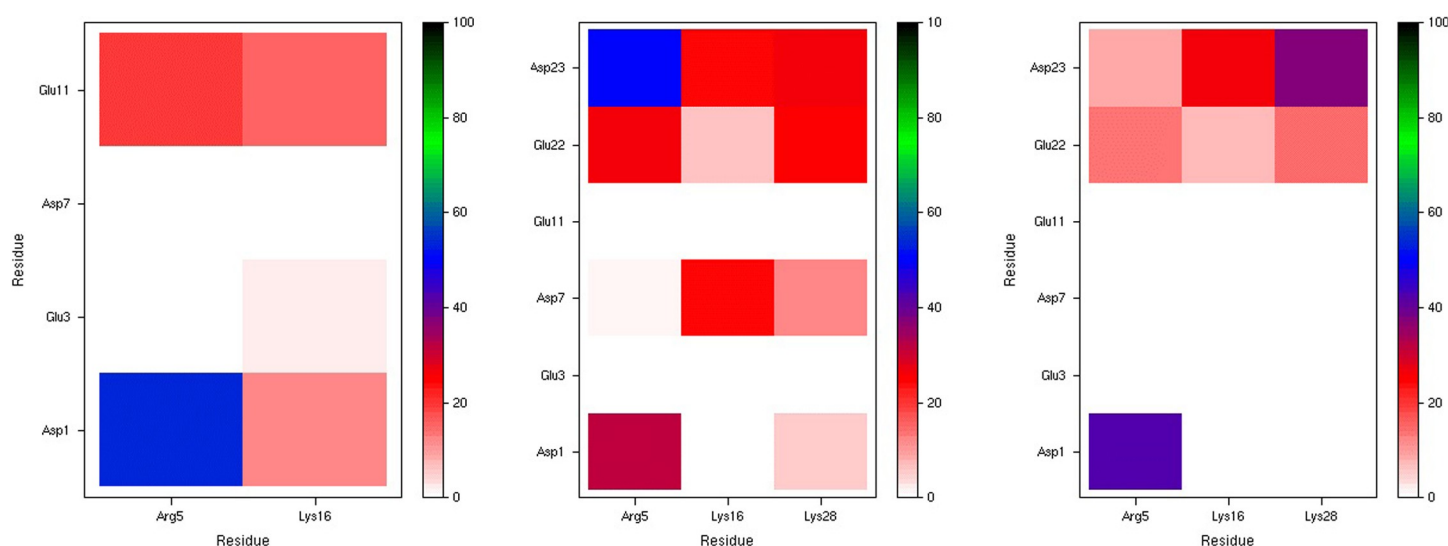


**Fig 8. Salt bridge incidence plots (%) for Al-Aβ16, Al-Aβ40 and Al-Aβ42 simulations.**

<https://doi.org/10.1371/journal.pone.0217992.g008>

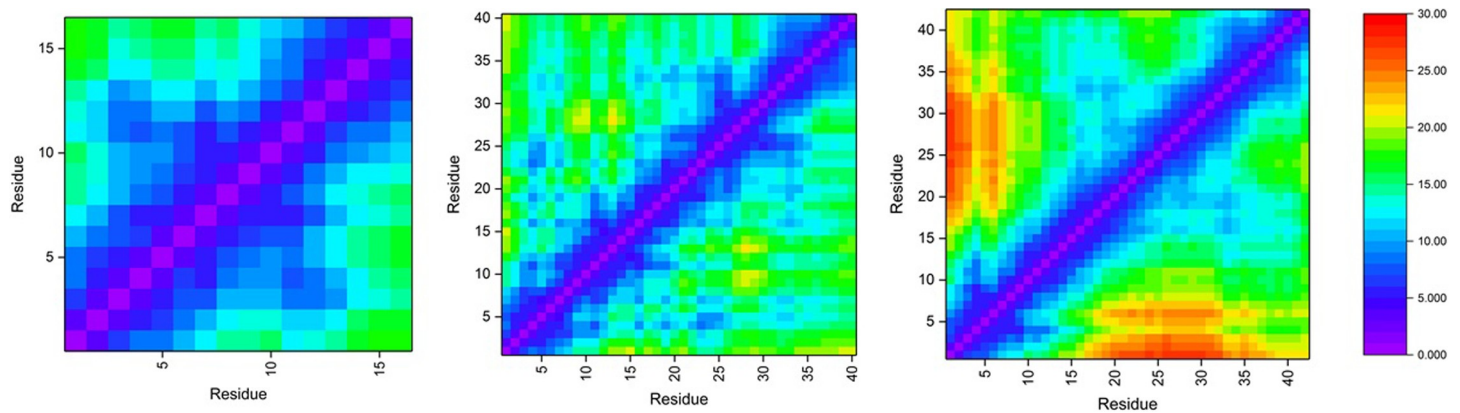


**Fig 9.**  $\alpha$ - $\alpha$  contact maps for Al-A $\beta$ 16, Al-A $\beta$ 40 and Al-A $\beta$ 42.

<https://doi.org/10.1371/journal.pone.0217992.g009>

occupation of the Asp1-Arg5 salt bridge. In contrast, salt bridge patterns beyond the N-terminus as well as the tertiary structure differ between Al-A $\beta$ 16 and the longer peptides.

Comparing Al-A $\beta$ 40 with Al-A $\beta$ 42 is instructive. The latter equilibrates to larger RMSD and Rg values, and the final two residues (Ile41 and Ala42) are particularly mobile in RMSF measurements. These residues adopt little secondary structure, Ala42 in particular remaining classified as coil throughout all trajectories, while Ile41 includes small amounts of turn, helical and sheet types. The presence of these unstructured, hydrophobic amino acids affects the pattern of salt bridges: Asp23-Lys28, known to be important in the conformational changes that accompany formation of fibrils,[49] is favoured over Asp23-Arg5, seen in Al-A $\beta$ 40. The flexible, hydrophobic residues and changed salt bridge pattern are reflected in the tertiary structures of A $\beta$ 40 and A $\beta$ 42, the latter adopting a more expanded set of conformations with particularly long distances between N-terminal residues and those between Phe20 and Ala30.

It also interesting to compare the trajectories reported here with those for the free A $\beta$ 42 and its adducts with Cu(II) and Pt(II)-phenanthroline, as reported by us recently.[48] Al(III) leads to structures that are larger than the free peptide (Rg = 9.6 Å) but smaller than Cu (13.8 Å) or Pt (16.5 Å) adducts, perhaps reflecting the harder nature of the small, highly charged Al(III) ion. Secondary structure, contact maps and salt bridge patterns are most similar to those observed for Cu(II) coordination, despite the fact that this ion binds through different residues (Ala2, His6, His13 and His14), suggesting that the identity of the metal ion and/or

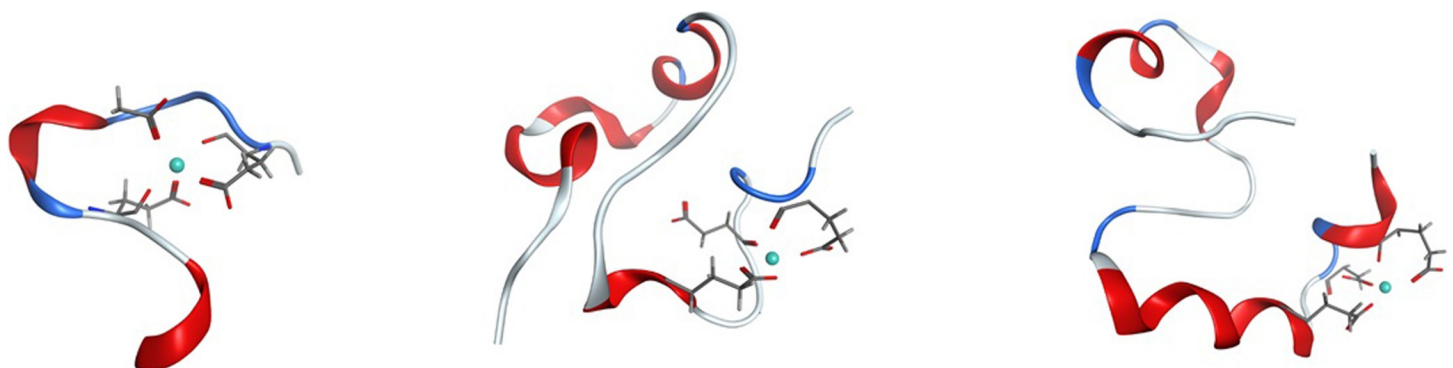


**Fig 10.** Most populated clusters for Al-A $\beta$ 16, Al-A $\beta$ 40 and Al-A $\beta$ 42 simulations. Al(III) is shown as a cyan sphere, selected atoms of Glu3, Asp7 and Glu11 as wireframe, and the remainder of the peptide as a ribbon, coloured by secondary structure (red = helix, blue = turn, white = coil).

<https://doi.org/10.1371/journal.pone.0217992.g010>

coordinating residues are less important than the presence/absence of a ligand free ion bound to the N-terminal region of A $\beta$ 42.

## Conclusions

Our data show that atomistic molecular dynamics simulations of Al(III) bound to amyloid- $\beta$  peptides of different lengths, using a non-bonded model of ion coordination, equilibrate in timescales of several hundred nanoseconds. Collating post-equilibration trajectories from multiple microsecond MD runs indicates stable binding of Al(III) to acidic residues in the N-terminal region of A $\beta$  and an average coordination number of around 4. The metal binding residues Glu3, Asp7 and Glu11 are typically relatively immobile, while N- and C-terminal residues are highly flexible. This flexibility still allows significant quantities of secondary structure to develop: the longest peptide, A $\beta$ 42, reaches almost 50% helical content, this being concentrated largely in residues 11–20 and 26–36. Salt bridges are strongly affected by the presence of the ion, most notably as coordination to acidic N-terminal residues severely retards their ability to form salt bridges. This, along with hydrogen bond patterns that reflect the rather high helical content, leads to characteristic patterns in tertiary structure in which stable contacts between salt bridged pairs, as well as residues bound to Al(III) are apparent. Overall, we find that coordination of Al(III) to the N-terminus of A $\beta$  has a major impact in the structure and dynamics of the peptide, inducing significant helical content, reducing the impact of salt bridges, reducing the flexibility of binding residues and increasing that of terminal residues.

## Supporting information

**S1 Fig. RDF and integrated RDF of Al-oxygen distances in Al-A $\beta$ 16.**  
(DOCX)

**S2 Fig. RDF and integrated RDF of Al-oxygen distances in Al-A $\beta$ 40.**  
(DOCX)

**S1 Table. RMSD data for individual MD runs.**  
(DOCX)

**S2 Table. RMSF by residue.**  
(DOCX)

**S3 Table. Salt bridge incidences (%).**  
(DOCX)

## Acknowledgments

We are grateful to Cardiff University's ARCCA facility for access to high-performance computing resources.

## Author Contributions

**Conceptualization:** Matthew Turner, Shaun T. Mutter, James A. Platts.

**Data curation:** Matthew Turner, James A. Platts.

**Formal analysis:** Matthew Turner, James A. Platts.

**Funding acquisition:** James A. Platts.

**Investigation:** Matthew Turner, James A. Platts.



**Methodology:** Matthew Turner, Shaun T. Mutter, Oliver D. Kennedy-Britten, James A. Platts.

**Project administration:** James A. Platts.

**Resources:** Matthew Turner, James A. Platts.

**Software:** Matthew Turner, James A. Platts.

**Supervision:** James A. Platts.

**Validation:** Matthew Turner, James A. Platts.

**Visualization:** Matthew Turner, Shaun T. Mutter, Oliver D. Kennedy-Britten, James A. Platts.

**Writing – original draft:** Matthew Turner, James A. Platts.

**Writing – review & editing:** Matthew Turner, Shaun T. Mutter, Oliver D. Kennedy-Britten, James A. Platts.

## References

1. Hardy J, Higgins G. Alzheimers-Disease—the Amyloid Cascade Hypothesis. *Science*. 1992; 256: 184–185. <https://doi.org/10.1126/science.1566067> PMID: [1566067](#)
2. Hardy J. Alzheimer's disease: The amyloid cascade hypothesis: An update and reappraisal. *J Alzheimers Dis*. 2006; 9: 151–153. <https://doi.org/10.3233/JAD-2006-9S317> PMID: [16914853](#)
3. Kepp K. Bioinorganic Chemistry of Alzheimer's Disease. *Chem Rev*. 2012; 112: 5193–5239. <https://doi.org/10.1021/cr300009x> PMID: [22793492](#)
4. Kepp K. Alzheimer's disease: How metal ions define  $\beta$ -amyloid function. *Coord Chem Rev*. 2017; 351: 127–159. <https://doi.org/10.1016/j.ccr.2017.05.007>
5. Faller P, Hureau C. Metal ions in neurodegenerative diseases. *Coord Chem Rev*. 2012; 256: 2127–2128. <https://doi.org/10.1016/j.ccr.2012.04.006>
6. Mold M, Ouro-Gnao L, Wieckowski BM, Exley C. Copper prevents amyloid- $\beta_{1-42}$  from forming amyloid fibrils under near-physiological conditions *in vitro*. *Sci Rep*. 2013; 3: 1256. <https://doi.org/10.1038/srep01256> PMID: [23409247](#)
7. Sarell CJ, Syme CD, Rigby SEJ, Viles JH. Copper(II) Binding to Amyloid- $\beta$  Fibrils of Alzheimer's Disease Reveals a Picomolar Affinity: Stoichiometry and Coordination Geometry Are Independent of A $\beta$  Oligomeric Form. *Biochemistry*. 2009; 48: 4388–4402. <https://doi.org/10.1021/bi900254n> PMID: [19338344](#)
8. Syme CD, Nadal RC, Rigby SEJ, Viles JH. Copper Binding to the Amyloid- $\beta$  (A $\beta$ ) Peptide Associated with Alzheimer's Disease. Folding, Coordination Geometry, pH Dependence, Stoichiometry, and Affinity of A $\beta$ -(1–28): Insights from a Range of Complementary Spectroscopic Techniques. *J Biol Chem*. 2004; 279: 18169–18177. <https://doi.org/10.1074/jbc.M313572200> PMID: [14978032](#)
9. Huy PDQ, Vuong QV, La Penna G, Faller P, Li MS. Impact of Cu(II) Binding on Structures and Dynamics of A $\beta$ 42 Monomer and Dimer: Molecular Dynamics Study. *ACS Chem Neurosci*. 2016; 7: 1348–1363. <https://doi.org/10.1021/acschemneuro.6b00109> PMID: [27454036](#)
10. Furlan S, Hureau C, Faller P, La Penna G. Modeling the Cu+ Binding in the 1–16 Region of the Amyloid- $\beta$  Peptide Involved in Alzheimer's Disease. *J Phys Chem B*. 2010; 114: 15119–15133. <https://doi.org/10.1021/jp102928h> PMID: [21038888](#)
11. De Gregorio G, Biasotto F, Hecel A, Luczkowski M, Kozłowski H, Valensin D. Structural analysis of copper(I) interaction with amyloid  $\beta$  peptide. *J Inorg Biochem*. 2019; 195: 31–38. <https://doi.org/10.1016/j.jinorgbio.2019.03.006> PMID: [30884319](#)
12. Faller P, Hureau C. Bioinorganic chemistry of copper and zinc ions coordinated to amyloid- $\beta$  peptide. *Dalton Trans*. 2009; 0: 1080–1094. <https://doi.org/10.1039/B813398K> PMID: [19322475](#)
13. Giannozzi P, Jansen K, La Penna G, Minicozzi V, Morante S, Rossi G, et al. Zn induced structural aggregation patterns of beta-amyloid peptides by first-principle simulations and XAS measurements. *Metallomics*. 2012; 4: 156–165. <https://doi.org/10.1039/c2mt00148a> PMID: [22170501](#)
14. Kozin SA, Zirah S, Rebuffat S, Hui Bon Hoa G, Debey P. Zinc Binding to Alzheimer's A $\beta$ (1–16) Peptide Results in Stable Soluble Complex. *Biochem Biophys Res Commun*. 2001; 285: 959–964. <https://doi.org/10.1006/bbrc.2001.5284> PMID: [11467845](#)

15. Zirah S, Kozin SA, Mazur AK, Blond A, Cheminant M, Segalas-Milazzo I, et al. Structural changes of region 1–16 of the Alzheimer disease amyloid beta-peptide upon zinc binding and in vitro aging. *J Biol Chem*. 2006; 281: 2151–2161. <https://doi.org/10.1074/jbc.M504454200> PMID: 16301322
16. Bousejra-ElGarah F, Bijani C, Coppel Y, Faller P, Hureau C. Iron(II) Binding to Amyloid- $\beta$ , the Alzheimer's Peptide. *Inorg Chem*. 2011; 50: 9024–9030. <https://doi.org/10.1021/ic201233b> PMID: 21800824
17. Kozlowski H, Luczkowski M, Remelli M, Valensin D. Copper, zinc and iron in neurodegenerative diseases (Alzheimer's, Parkinson's and prion diseases). *Coord Chem Rev*. 2012; 256: 2129–2141. <https://doi.org/10.1016/j.ccr.2012.03.013>
18. Lovell MA, Robertson JD, Teesdale WJ, Campbell JL, Markesbery WR. Copper, iron and zinc in Alzheimer's disease senile plaques. *J Neurol Sci*. 1998; 158: 47–52. [https://doi.org/10.1016/S0022-510X\(98\)00092-6](https://doi.org/10.1016/S0022-510X(98)00092-6) PMID: 9667777
19. Boopathi S, Kolandaivel P. Fe<sup>2+</sup> binding on amyloid  $\beta$ -peptide promotes aggregation. *Proteins Struct Funct Bioinforma*. 2016; 84: 1257–1274. <https://doi.org/10.1002/prot.25075> PMID: 27214008
20. Strodel B, Coskuner-Weber O. Transition Metal Ion Interactions with Disordered Amyloid- $\beta$  Peptides in the Pathogenesis of Alzheimer's Disease: Insights from Computational Chemistry Studies. *J Chem Inf Model*. 2019; <https://doi.org/10.1021/acs.jcim.8b00983> PMID: 30933519
21. Exley C. The coordination chemistry of aluminium in neurodegenerative disease. *Coord Chem Rev*. 2012; 256: 2142–2146. <https://doi.org/10.1016/j.ccr.2012.02.020>
22. House E, Collingwood J, Khan A, Korchazkina O, Berthon G, Exley C. Aluminium, iron, zinc and copper influence the in vitro formation of amyloid fibrils of A $\beta$ 42 in a manner which may have consequences for metal chelation therapy in Alzheimer's disease. *J Alzheimers Dis JAD*. 2004; 6: 291–301. PMID: 15201484
23. Kawahara M, Kato-Negishi M. Link between Aluminum and the Pathogenesis of Alzheimer's Disease: The Integration of the Aluminum and Amyloid Cascade Hypotheses. *Int J Alzheimers Dis*. 2011; 2011. <https://doi.org/10.4061/2011/276393> PMID: 21423554
24. Bolognin S, Messori L, Drago D, Gabbiani C, Cendron L, Zatta P. Aluminum, copper, iron and zinc differentially alter amyloid-A  $\beta$ (1–42) aggregation and toxicity. *Int J Biochem Cell Biol*. 2011; 43: 877–885. <https://doi.org/10.1016/j.biocel.2011.02.009> PMID: 21376832
25. Huang X, Atwood CS, Moir RD, Hartshorn MA, Tanzi RE, Bush AI. Trace metal contamination initiates the apparent auto-aggregation, amyloidosis, and oligomerization of Alzheimer's A $\beta$  peptides. *JBIC J Biol Inorg Chem*. 2004; 9: 954–960. <https://doi.org/10.1007/s00775-004-0602-8> PMID: 15578276
26. Exley C, Price NC, Kelly SM, Birchall JD. An interaction of beta-amyloid with aluminium in vitro. *FEBS Lett*. 1993; 324: 293–295. PMID: 8405368
27. Kawahara M, Muramoto K, Kobayashi K, Mori H, Kuroda Y. Aluminum Promotes the Aggregation of Alzheimer's Amyloid  $\beta$ -Protein in Vitro. *Biochem Biophys Res Commun*. 1994; 198: 531–535. <https://doi.org/10.1006/bbrc.1994.1078> PMID: 7507666
28. Mujika JI, Ruipérez F, Infante I, Ugalde JM, Exley C, Lopez X. Pro-oxidant activity of aluminum: stabilization of the aluminum superoxide radical ion. *J Phys Chem A*. 2011; 115: 6717–6723. <https://doi.org/10.1021/jp203290b> PMID: 21604694
29. Mujika JI, Dalla Torre G, Formoso E, Grande-Aztatzi R, Grabowski SJ, Exley C, et al. Aluminum's preferential binding site in proteins: sidechain of amino acids versus backbone interactions. *J Inorg Biochem*. 2018; 181: 111–116. <https://doi.org/10.1016/j.jinorgbio.2017.10.014> PMID: 29183625
30. Mujika JI, Rezabal E, Mercero JM, Ruipérez F, Costa D, Ugalde JM, et al. Aluminium in Biological Environments: A Computational Approach. *Comput Struct Biotechnol J*. 2014; 9: e201403002. <https://doi.org/10.5936/csbj.201403002> PMID: 24757505
31. Mujika JI, Rodríguez-Guerra Pedregal J, Lopez X, Ugalde JM, Rodríguez-Santiago L, Sodupe M, et al. Elucidating the 3D structures of Al(III)–A $\beta$  complexes: a template free strategy based on the pre-organization hypothesis. *Chem Sci*. 2017; 8: 5041–5049. <https://doi.org/10.1039/c7sc01296a> PMID: 28970891
32. Huraskin D, Horn AHC. Alkali ion influence on structure and stability of fibrillar amyloid- $\beta$  oligomers. *J Mol Model*. 2019; 25. <https://doi.org/10.1007/s00894-018-3920-4> PMID: 30637529
33. Molecular Operating Environment (MOE). 1010 Sherbooke St. West, Suite #910, Montreal, QC, Canada, H3A 2R7: Chemical Computing Group Inc.; 2013.
34. Labute P. LowModeMD—Implicit Low-Mode Velocity Filtering Applied to Conformational Search of Macrocycles and Protein Loops. *J Chem Inf Model*. 2010; 50: 792–800. <https://doi.org/10.1021/ci900508k> PMID: 20429574
35. Case DA, Betz RM, Cerutti DS, Darden TA, Duke RE, Giese TJ, et al. AMBER 2016. University of California, San Francisco; 2016.

36. Maier JA, Martinez C, Kasavajhala K, Wickstrom L, Hauser KE, Simmerling C. ff14SB: Improving the Accuracy of Protein Side Chain and Backbone Parameters from ff99SB. *J Chem Theory Comput.* 2015; 11: 3696–3713. <https://doi.org/10.1021/acs.jctc.5b00255> PMID: [26574453](#)
37. Li P, Merz KM. MCPB.py: A Python Based Metal Center Parameter Builder. *J Chem Inf Model.* 2016; 56: 599–604. <https://doi.org/10.1021/acs.jcim.5b00674> PMID: [26913476](#)
38. Frisch MJ, Trucks GW, Schlegel HB, Scuseria GE, Robb MA, Cheeseman JR, et al. Gaussian09. Wallingford, CT: Gaussian Inc.; 2009.
39. Onufriev A. Continuum Electrostatics Solvent Modeling with the Generalized Born Model. In: Feig M, editor. *Modeling Solvent Environments*. Weinheim, Germany: Wiley-VCH Verlag GmbH & Co. KGaA; 2010. pp. 127–165. <https://doi.org/10.1002/9783527629251.ch6>
40. Anandakrishnan R, Drozdetski A, Walker RC, Onufriev AV. Speed of Conformational Change: Comparing Explicit and Implicit Solvent Molecular Dynamics Simulations. *Biophys J.* 2015; 108: 1153–1164. <https://doi.org/10.1016/j.bpj.2014.12.047> PMID: [25762327](#)
41. Roe DR, Cheatham TE. PTRAJ and CPPTRAJ: Software for Processing and Analysis of Molecular Dynamics Trajectory Data. *J Chem Theory Comput.* 2013; 9: 3084–3095. <https://doi.org/10.1021/ct400341p> PMID: [26583988](#)
42. Humphrey W, Dalke A, Schulten K. VMD: visual molecular dynamics. *J Mol Graph.* 1996; 14: 33–38, 27–28. [https://doi.org/10.1016/0263-7855\(96\)00018-5](https://doi.org/10.1016/0263-7855(96)00018-5) PMID: [8744570](#)
43. Frishman D, Argos P. Knowledge-based protein secondary structure assignment. *Proteins-Struct Funct Genet.* 1995; 23: 566–579. <https://doi.org/10.1002/prot.340230412> PMID: [8749853](#)
44. Martin Ester H-PK, Jörg Sander XX. A Density-Based Algorithm for Discovering Clusters in Large Spatial Databases with Noise.
45. Margreitter C, Oostenbrink C. MDplot: Visualise Molecular Dynamics. *R J.* 2017; 9: 164–186. PMID: [28845302](#)
46. Mutter ST, Turner M, Deeth RJ, Platts JA. Metal Binding to Amyloid- $\beta$ 1–42: A Ligand Field Molecular Dynamics Study. *ACS Chem Neurosci.* 2018;(In press). <https://doi.org/10.1021/acschemneuro.8b00210> PMID: [29898363](#)
47. Wang L, Zeng R, Pang X, Gu Q, Tan W. The mechanisms of flavonoids inhibiting conformational transition of amyloid- $\beta$  42 monomer: a comparative molecular dynamics simulation study. *RSC Adv.* 2015; 5: 66391–66402. <https://doi.org/10.1039/C5RA12328C>
48. Turner M, Mutter ST, Platts JA. Molecular dynamics simulation on the effect of transition metal binding to the N-terminal fragment of amyloid- $\beta$ . *J Biomol Struct Dyn.* 2018; 1–11. <https://doi.org/10.1080/07391102.2018.1555490> PMID: [30526382](#)
49. Sciarretta KL, Gordon DJ, Petkova AT, Tycko R, Meredith SC. A $\beta$ 40-Lactam(D23/K28) Models a Conformation Highly Favorable for Nucleation of Amyloid. *Biochemistry.* 2005; 44: 6003–6014. <https://doi.org/10.1021/bi0474867> PMID: [15835889](#)